# First-principles study of noncommutative band offsets at $\alpha$-Cr$_2$O$_3$/$\alpha$-Fe$_2$O$_3$(0001) interfaces

John E. Jaffe,[1] Michel Dupuis,[1] and Maciej Gutowski[1,2,*]

[1]*Chemical Sciences Division, Fundamental Sciences Directorate, Pacific Northwest National Laboratory, Richland, Washington 99352, USA*

[2]*Department of Chemistry, University of Gdansk, 80-952 Gdansk, Poland*

Using first-principles density functional theory, we have modeled the atomic, electronic and magnetic structure of epitaxial interfaces between alpha-hematite and alpha-chromia (corundum structure) in the hexagonal (0001) basal plane. Our model was a superlattice with a period of about 27.5 Å, corresponding to the shortest-period superlattice considered in a recent series of experiments [Chambers *et al.*, Phys. Rev. B **61**, 13223 (2000)]. Two different epitaxial interface structures were studied: (*i*) an oxygen plane separating an Fe double layer from a Cr double layer or (*ii*) a metal double layer split between Fe and Cr. We found that these two structures are close in total energy but have distinct spin structure and different valence band offsets [chromia above hematite by 0.4 and 0.6 eV for (*i*) and (*ii*), respectively], possibly explaining the experimental noncommutative band offset seen in this system ($0.3\pm0.1$ eV for hematite grown atop chromia, and $0.7\pm0.1$ eV for the reverse).

## I. INTRODUCTION

Metal oxides have played a prominent role for many years in chemistry as heterogeneous catalysts or catalyst support structures, but they have traditionally played a more secondary role in electronic and opto-electronic devices as substrates, insulators, gate dielectrics, window materials or protective coatings. Recently, however, oxides have emerged as possible key active elements in a new generation of devices. Transition metal oxides[1] in particular, whether binary, ternary or more complex, have an especially rich set of properties, ranging from high dielectric constants and ferroelectricity to magnetic order and high-temperature superconductivity. Devices combining two or more oxide materials as active regions permit even more possibilities, including band-gap, photonic and spin-transport engineering of superlattices, interfaces and surfaces.

An example of such a device was described in a recent paper[2] in which epitiaxial (0001) superlattices of hematite ($\alpha$-Fe$_2$O$_3$) and chromia (eskolaite, $\alpha$-Cr$_2$O$_3$) were grown by oxygen-plasma-assisted molecular beam epitaxy (OPA-MBE) on sapphire ($\alpha$-Al$_2$O$_3$) substrates. These superlattices showed a remarkable "band-offset noncommutativity" in which the valence band offset between the two materials differed according to which one was grown on top: $0.3\pm0.1$ eV for hematite grown atop chromia and $0.7\pm0.1$ eV for chromia grown atop hematite, where in the present notation a positive offset means chromia has the higher (less deeply bound) valence band maximum. This behavior raised the possibility of a spontaneous average electric potential gradient across several periods of the superlattice. Such a structure could efficiently separate electron and holes in, for example, a photoelectrochemical device. Interesting magnetic effects might also occur due to the differing antiferromagnetic order in hematite and chromia. However, the interface structure that causes the asymmetry in band offsets is unknown.

In an effort to understand these unusual properties of the $\alpha$-Fe$_2$O$_3$/$\alpha$-Cr$_2$O$_3$ interface, we have performed density functional calculations on a model superlattice corresponding to one hexagonal unit cell each of the two oxides, or 36 atomic layers in a unit cell (counting each metal bilayer as two layers.) We find that two distinctly different interface structures are possible, depending on whether there are metal bilayers split between Fe and Cr at the interface, or oxygen planes dividing the Cr from the Fe bilayers nearest to the interface. Though close in energy, these two structures indeed turned out to have different band offsets and distinct spin and electronic structure, raising novel possibilities for device construction. This work is, to our knowledge, the first computational study of this interfacial *mixed* oxide system, though we note that there have been several theoretical works on bulk and surfaces of hematite[3] and chromia[4] in recent years.

We describe our computational approach and the details of our model system in Secs. II and III below, with the main body of our results in Sec. IV and further discussion in Sec. V, followed by a summary.

## II. COMPUTATIONAL METHODOLOGY

Using first-principles density functional theory (DFT) and ultrasoft pseudo-potentials, we modeled the atomic, electronic and magnetic structure of epitaxial interfaces between hematite and chromia (both having the corundum structure) in the hexagonal (0001) basal plane. We performed these calculations within the generalized gradient approximation[5] (PW91-GGA) using the Vienna Ab-initio Simulation Package (VASP).[6] For the geometry optimization (energy minimization), total energy calculations and characterization of the electronic and spin structure, we expanded the eigenstates in plane-wave basis functions and represented the ion cores with ultrasoft pseudopotentials.[7] The calculations were performed at relatively high levels of precision, for example

a kinetic energy cutoff of 396 eV was used for the plane wave basis.

We calculated the band offsets between $Fe_2O_3$ and $Cr_2O_3$ by a variant of a standard method in semiconductor theory.[8] The band offset, or difference between the valence band maxima of two semiconductors or insulators, cannot simply be taken as the difference between their highest occupied eigenstates in bulk band structure calculations, because there is not in general any correspondence between the "zero of energy" of one-electron levels in two such calculations for different materials. Instead, the standard scheme is to construct a superlattice of the two materials with a well-defined interface between them. Next a reference level (a core eigenvalue or average electrostatic potential) is calculated in the interior or "bulk-like" regions of the two materials (that is, not "too close" to the interface, so the superlattice period must be of sufficient size.) Next, the same two reference levels are calculated with respect to the valence band maxima of the two materials in separate bulk calculations. Finally, these valence band maxima are shifted by the difference between the reference levels in the bulk and superlattice calculations, and their difference then taken to obtain the valence band offset. The band gap difference between the two bulk materials (often taken directly from experiment) is then added the valence band offset to obtain the conduction band offset.

It is clear that the band offsets will depend on the particular interface chosen as well as on the electronic structure of each material *per se*. In the present case, using the subscripts $F$ for $Fe_2O_3$ and $C$ for $Cr_2O_3$, we may express the valence band offset between these oxides as

$$\Delta E_{F-C}^{V} = E_{F,bulk}^{V} - E_{F,bulk}^{core} - (E_{C,bulk}^{V} - E_{C,bulk}^{core})$$
$$+ E_{F,superlattice}^{core} - E_{C,superlattice}^{core}, \tag{1}$$

where $E_{F,bulk}^{V}$ is the calculated bulk valence band maximum for hematite, $E_{F,bulk}^{core}$ is a core reference level or average core potential in bulk hematite, $E_{F,superlattice}^{core}$ is the same reference level calculated for an interior layer in the hematite region of the superlattice, and the other terms are defined analogously for chromia. In our calculation of band offsets, we used the average core electrostatic potentials calculated in the VASP code as reference levels. These core potentials of course contain some intra-atomic effects, but added to this is the electrostatic potential due to the atom's environment, and the change in this added term remains when we subtract the core potential for an atom of the same element in the other environment.

More commonly in plane-wave band offset calculations, a coarse-grained spatial average electrostatic potential is used as a reference. To make sure that our approach agrees with the standard one, we calculated the band offset for an eight-atomic-layer zinc-blende AlN/GaN (001) superlattice. We found a valence band offset of 0.84 eV (GaN above AlN) from an average of the N and cation core potential differences between the bulk compounds and the central layer of each zone (GaN or AlN) in the superlattice, in nearly exact agreement with the results[8] from spatial averaging. Using

only nitrogen atom or only cation core potential shifts, our calculated band offsets were 0.78 and 0.91 eV, respectively, still in very good agreement with the published result. This gives us confidence that the average core potentials are an accurate as well as convenient proxy for the potential difference created by local polarization at the "distant" interface.

One further methodological question is how to rationally partition the electronic charge among all the atoms in order to realistically characterize the charge redistribution accompanying interface formation. When plane-wave codes are used, a common practice is to integrate the charges within nucleus-centered spheres to obtain atomic charge and spin populations. These spheres are often also used to decompose the total density of states into atomic and "orbital" projected density of states. The radii of these spheres are usually taken from some set of "touching" radii, such as a standard set of covalent radii, and then scaled so that the sum of sphere volumes equals the actual total volume of the unit cell. This approach does not in general keep the sum of all atomic charges equal to the exact charge of the unit cell, because it double-counts electronic charge near the interatomic bonds (where the spheres may overlap) while neglecting some of the interstitial spaces. There is also no guarantee that the sphere radii used are at all reasonable for the system under study. It would be useful to continue using the simple sphere-integration scheme while deriving a set of sphere radii from the calculated charge density that contain information about the nature of the bonding (degree of ionic or covalent character) while minimizing the error in the total charge. For most solids, the bonding is neither purely ionic nor covalent, so an adaptive approach should be better than using a set of arbitrary radii valid only in the ionic or covalent limit.

Hence we proposed a simple method to adapt the radii to the actual charge distribution in the material under study while maintaining the "volume sum rule" and minimizing the difference between the actual number of electrons in the unit cell and the electronic charge that is accounted for inside the spheres.[9] We vary the oxygen radius while adjusting the metal atom radius to enforce the volume sum rule, and note the value of the total charge that results from summing the integrated charges in every sphere. In each case the total charge has a single maximum with a value near the correct number of valence electrons in the unit cell. We take the radii corresponding to the position of this maximum as the appropriate set of atomic radii for the structure under consideration. The resulting radii are reasonable in that they are between typical ionic and covalent radii, as expected for systems of mixed bonding character. Another benefit of this approach is that the atomic-sphere-projected densities of states sum accurately to equal the total density of states.

### III. CHOICE OF MODEL SYSTEMS

Our model was a superlattice with a period of about 27.5 Å, with six double (puckered) layers ("bilayers") of Cr followed by six similar double layers of Fe, with successive metal bilayers separated by oxygen planes, for a total of 60 atoms per unit cell. This model corresponds to the shortest of several superlattice periods considered in Ref. 2. The initial
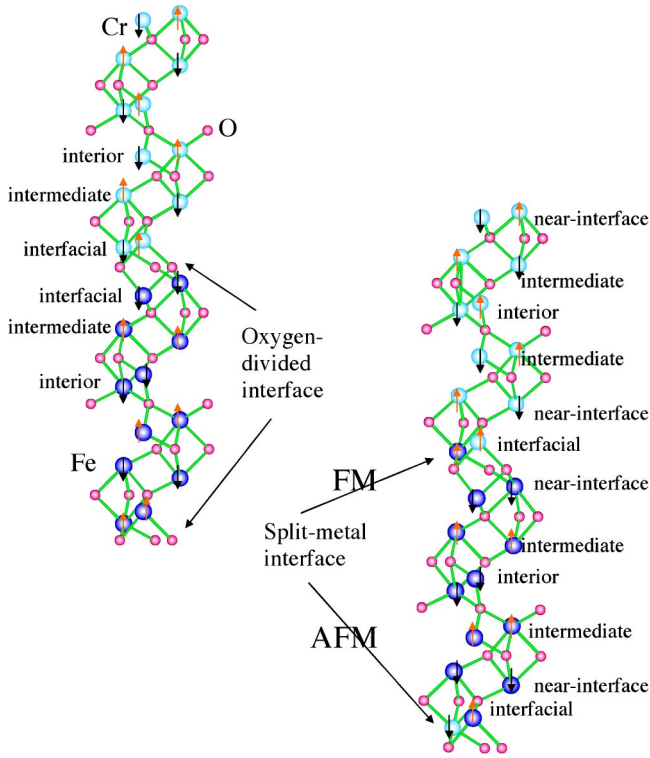
FIG. 1. (Color online) Interface supercell structures for (a) the oxygen-divided and (b) the split-metal interfaces between $\alpha$-Fe$_2$O$_3$ (bottom part of the supercell) and $\alpha$-Cr$_2$O$_3$ (upper part of the supercell). The Fe and Cr ions marked with dark and light gray circles, respectively. The interface planes and various layers discussed in the text are indicated, as well as the majority spin direction of each metal atom.

atomic positions for the supercells with interfaces were obtained by stacking two complete hexagonal unit cells of the corundum structure, one of Fe$_2$O$_3$ and one of Cr$_2$O$_3$, with the lattice constants in the (0001) plane set to an average of those of the two pure materials. Apart from the change in chemical composition at the interface, we assumed that the stacked cells were not initially rotated in relation to each other or displaced parallel to the interface, and that the interface was perfectly epitaxial, i.e., the two-dimensional periodicity with respect to the interface plane is the same on both sides of the interface.

In view of the noncommutative character of the Cr$_2$O$_3$/Fe$_2$O$_3$ interface[2] we considered various atomic structures for the epitaxial interfaces. We recognized that two distinct interfaces are possible: an oxygen layer may divide an Fe bilayer from a Cr bilayer, or alternatively there may be a bilayer at the interface that is split into an Fe layer and a Cr layer. We call these structures the "oxygen-divided" (OD) and "split-metal" (SM) interfaces, respectively; the unit cells containing these interfaces are shown in Fig. 1.

## IV. RESULTS OF CALCULATIONS

### A. Bulk Fe$_2$O$_3$ and Cr$_2$O$_3$

We began by calculating the bulk structural parameters of $\alpha$-Fe$_2$O$_3$ (hematite), $\alpha$-Cr$_2$O$_3$ (eskolaite), and (as a refer-

TABLE I. Rhombohedral lattice constants and bulk modulus of hematite, chromia (Eskolaite) and corundum.

|  | $a_{calc}$(Å) | $a_{expt}$(Å) | $\alpha_{calc}$ | $\alpha_{expt}$ | $B_{calc}(GPa)$ | $B_{expt}(GPa)$ |
|---|---|---|---|---|---|---|
| Fe$_2$O$_3$ | 5.436 | 5.412 | 55.00° | 55.38° | 181 | 230 |
| Cr$_2$O$_3$ | 5.391 | 5.378 | 54.32° | 54.44° | 218 | 240 |
| Al$_2$O$_3$ | 5.161 | 5.129 | 55.30° | 55.30° | 223 | 250 |

ence for accuracy) $\alpha$-Al$_2$O$_3$ (corundum) by total energy minimization; the results, as Table I shows, are in excellent agreement with experiment.

We also confirmed that the antiferromagnetic (AFM) order known to exist experimentally[10] in each of the transition metal compounds has the lowest energy in our calculations as well. In Cr$_2$O$_3$ the spins order antiferromagnetically both in the metal bilayers in the basal plane, and also normal to them. In Fe$_2$O$_3$ they order antiferromagnetically in the normal direction but ferromagnetically within the bilayers. Of these two AFM orderings, plus a ferromagnetic (FM) and a nonmagnetic, spin-restricted state, the experimentally correct AFM order[10] is found in each case to have the lowest energy. The calculated FM-AFM energy difference is much larger for hematite than for chromia, consistent with the much higher Néel temperature[1] of Fe$_2$O$_3$.

Our charge-partitioning scheme led to atomic radii of $R_{Fe}$= 1.55 Å and $R_O$= 1.15 Å in Fe$_2$O$_3$, and $R_{Cr}$= 1.56 Å and $R_O$= 1.10 Å in Cr$_2$O$_3$. We have used these radii to calculate projected densities of states (PDOS) for bulk hematite and chromia as shown in Figs. 2(a) and 2(b), respectively. In the energy range shown, the only states with significant weight are those with $2p$ character within the O-centered spheres, and $3d$ character in the metal-centered spheres. This energy range encompasses the upper valence bands and lowest set of conduction bands. Only the spin-up direction is shown since when the entire antiferromagnetic bulk unit cells are considered, the up- and down-spin wave functions are related by symmetry. The zero of energy is the essentially arbitrary zero of the VASP eigenvalue scale, and has not been shifted in Fig. 2. There is a very significant degree of $p$-$d$ hybridization, more so for hematite than for chromia, as evidenced by the fact that the highest set of occupied bands is not pure metal $d$ in character. We also observe that chromia has a wider band gap and also apparently a higher valence band maximum, though the latter is not certain at this point since there is no necessary relation between the zeroes of single-electron energies in the band structures of these two different materials. However, we shall see below that this relation indeed holds true when the two compounds are interfaced, and that they therefore form a Type II heterojunction. (Type I corresponds to the case where the band gap of one material lies entirely within the gap of the other, Type II to the case where the gaps only partly overlap.)

### B. Interface atomic and magnetic structure

The static geometry optimization for the superlattice was started from bulk-like structures for the Fe$_2$O$_3$ and Cr$_2$O$_3$ layers. We also took the initial spin configuration from the
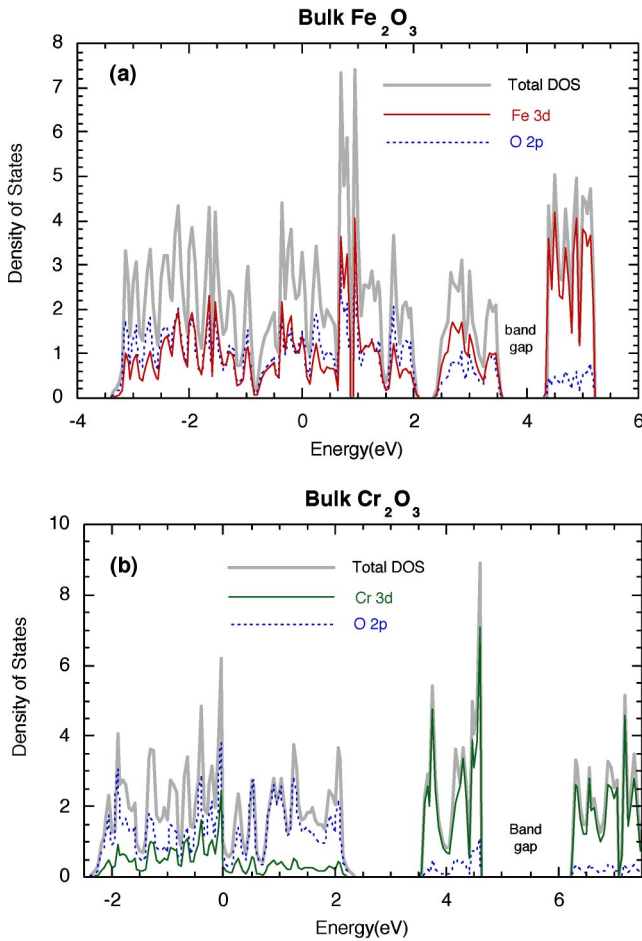
FIG. 2. (Color online) Total and projected (oxygen $2p$ and metal $3d$) density of states for (a) bulk $\alpha$-$Fe_2O_3$ and (b) bulk $\alpha$-$Cr_2O_3$.

bulk antiferromagnetic orderings known to exist in these systems, which are different in the two materials, as mentioned above. When we relaxed all atomic positions to an energy minimum, only fairly small (less than about 0.02 Å) displacements of the atomic positions resulted. The final atomic positions are those shown in Fig. 1. Though not constrained to remain in the same magnetic state throughout the electronic and atomic relaxation, the bulk magnetic order within the regions of each oxide did in fact remain unchanged in every case. The majority spin directions of all the atoms were also shown in Fig. 1.

The energy of the interface is defined by subtracting the energy of one hexagonal (three primitive) cell of each bulk oxide from the total energy of our $Fe_2O_3/Cr_2O_3$ unit cell. The resulting fully relaxed interfacial energies are 0.56 and 0.72 eV per unit cell for the split-metal and O-divided cells, respectively, or 13 and 17 meV/Å$^2$. These energies are about one order of magnitude smaller than typical *surface* energies of oxides and semiconductors. The structural relaxation upon interface formation lowered the interface energy by 9.7 and 14 meV/Å$^2$ for the SM and OD interfaces, respectively, so that relaxation lowered the interface energy by slightly less than a factor of 2, similar to the ratio for relaxed (or reconstructed) and unrelaxed surface energies in many cases. The relaxation also caused only small changes in nearest neigh-

bor distances on the order of 0.01 Å. The displacements were mostly along the hexagonal $c$-axis and the only significant trend in them was a small compression in the $Cr_2O_3$ region and a slight expansion of the $Fe_2O_3$ region. The interface supercell lattice constants themselves were also allowed to relax to an energy minimum, but there was little change in $c$ (it remained at essentially $c_{Fe_2O_3}+c_{Cr_2O_3}$) while the in-plane lattice constant[11] $a$ assumed a value intermediate between the values $a_{Fe_2O_3}=5.022$ Å and $a_{Cr_2O_3}=4.952$ Å; we obtained $a=4.986$ Å for the split-metal and $a=4.993$ Å for the oxygen-divided interfaces, respectively. This is in apparent disagreement to the experimental observation[2] that the $Cr_2O_3$ in-plane lattice constant apparently adjusted itself to equal the in-plane lattice constant of hematite. However, more recent measurements indicate that the $Cr_2O_3$ layers may not fully accommodate the $Fe_2O_3$ in-plane periodicity.[12] Our result is reasonable in that the bulk moduli shown in Table I for hematite and chromia are similar, so we would not expect to find one of them nearly unstrained while the other fully accommodates the first material's lattice constant.

A significant feature of these two chemically distinct interface structures is their effect on the antiferromagnetic spin order at the interface. As can be seen from Fig. 1, all the metal bilayers in the oxygen-divided supercell have the bulk hematite or chromia spin order, while in the split-metal supercell the interfacial metal bilayers are alternately ferro- and antiferromagnetic. This means that either the interfacial Cr or the interfacial Fe atom, respectively, is "frustrated." This spin frustration shows up to a small extent in the magnitude of the net spin population of atoms near the interface, in particular the Cr atom aligned ferromagnetically to a coplanar Fe at the split-metal interface has a spin population of 2.68 spins versus an average of 2.77 for all the Cr atoms in that unit supercell.

## C. Superlattice and interface electronic structure

In Fig. 3 we show the total density of states for both spin directions for (a) the oxygen divided and (b) the split-metal interfacial supercells. We also show the projected density of states summed over all atoms and angular momentum states ($s$, $p$, $d$) for the atoms in each half of the supercell, corresponding to six formula units of each of the two oxides. For both interfaces, we observe that the occupied states derived from hematite have very little weight in the top $\sim 0.5$ eV of the valence band, the states there being almost completely associated with the chromia half of the cell. In contrast, the states derived from chromia have very little weight in the bottom of the conduction band, the states there being almost completely associated with the hematite half of the cell. We also notice that the band gaps are smaller for both interfaces than for bulk hematite (see Figs. 2 and 3). All these features are consistent with the proposition[2] that $Cr_2O_3/Fe_2O_3$ is a Type II heterojunction.

We also observe that while the oxygen-divided density of states is almost perfectly symmetrical with respect to spin, the split-metal density of states shows large deviations from spin symmetry (though when integrated over energy, it still gives equal-spin pairing.) This asymmetry is a manifestation
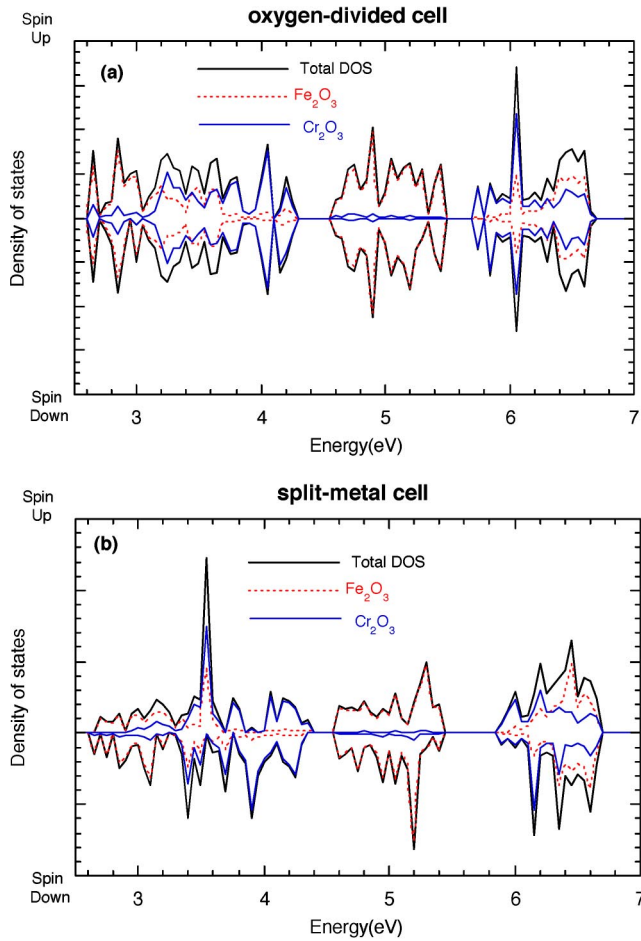
FIG. 3. (Color online) Total density of states for the interfacial supercells of Fig. 1, and projected density of states for all atoms in the $Fe_2O_3$ and $Cr_2O_3$ half-cells; (a) oxygen-divided and (b) split-metal.



FIG. 4. (Color online) Comparison of projected density of states for interior layers (furthest from interface) of $Fe_2O_3$ and $Cr_2O_3$ in the interfacial superlattice, with corresponding bulk density of states, shifted in energy by the difference in average core potentials between interior layers and bulk; (a) oxygen-divided and (b) split-metal. Each layer comprises a metal bilayer and its two adjoining oxygen planes (three atoms in each plane) with the oxygens weighted at 0.5 each to keep each layer at the $M_2O_3$ stoichiometry.

of the spin frustration discussed above; in particular, the ferromagnetic split-metal interfaces in our unit cell are either all spin-up as shown or all spin-down, so the two spin directions are no longer equivalent, even though there is zero net ferromagnetic moment when the total DOS is integrated over energy.

To further examine the electronic structure, we now consider the projection of the density of states onto individual layers in the superlattice. By a ''layer'' in this context, we mean a metal bilayer plus the oxygen atoms in the two adjoining oxygen planes, weighted at 50% to prevent double counting of oxygens as we go from one layer to the next. Including the oxygen atoms in the projection insures that even with the strong O $2p$-metal $3d$ hybridization, each group of bands will have the proper amplitude in the density of states. We first consider the density of states of the superlattice projected onto the interior layers of the hematite and chromia regions, that is, the layers furthest from the interface. We shift the energy zero for the total density of states of the pure bulk oxides by the difference in average core potentials between the interior layers and the bulk oxides, similar to what is done to the bulk valence band maxima in Eq. (1). In other words we line up the inner layer and bulk DOS by
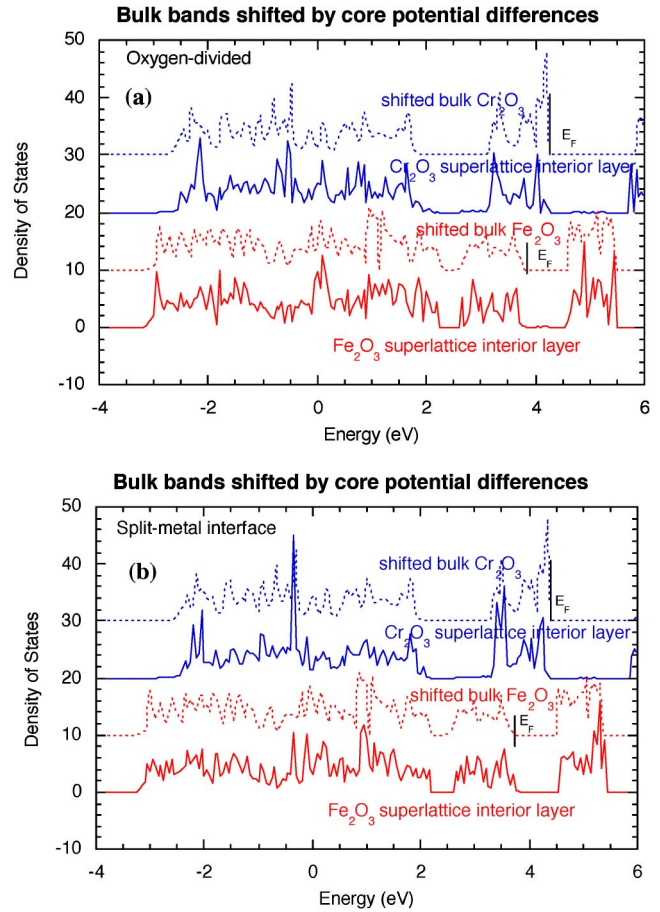
aligning their core potentials, as shown in Fig. 4 for (a) O-divided and (b) split-metal cells. We see from Fig. 4 that the bulk and interior layer DOS peaks can indeed be lined up quite closely, and the various features in the DOS have rather similar form for the bulk oxides and the interior layers in the superlattice. This indicates that these interior layers are indeed very bulk-like in character.

We now proceed to calculate the valence band offsets according to Eq. (1), using average core potentials from the ''interior'' layers in the hematite and chromia regions of the split-metal and O-divided cells, as marked in Fig. 1. With the electrostatic core potentials at the O atoms as the reference levels, we obtain 0.5 and 0.7 eV for the valence band offset (chromia higher than hematite) for the O-divided and split-metal interfaces, respectively. When the appropriate metal atom core potentials are used, these calculated offsets drop to 0.3 and 0.5 eV. Following the same procedure tested for AlN/GaN, when we average over both metal and oxygen core potential differences, we obtain 0.4 eV (O-divided) and 0.6 eV (split-metal) for the band offsets. We will take the

averaged values 0.4 and 0.6 eV as the most representative values in the discussion below, since band offsets are mostly controlled by long-ranged electrostatic potentials originating near the interfaces, and averaging over the potential changes at all the atoms in the interior layer helps to remove any perturbations due to purely local effects. Thus, the band offsets for the two interfaces are significantly different.

An important question remains, namely the extent to which our findings are sensitive to the interfacial in-plane strain. The results reported above were obtained for the fully relaxed supercells characterized in Fig. 1. We found, however, that the band offset for the split-metal interface changes by $+0.01$ and $+0.03$ eV when the values of the hexagonal $a$ and $b$ lattice constants are instead fixed to the bulk values for $Cr_2O_3$ and $Fe_2O_3$, respectively. Analogous modifications of the band offset value for the oxygen-divided interface are $-0.03$ and $+0.02$ eV. All these modifications are smaller by one order of magnitude than the difference in the band offset values for the split-metal and oxygen-divided interfaces. We conclude that the interfacial in-plane strain resulting from the lattice mismatch between $Cr_2O_3$ and $Fe_2O_3$ does not significantly affect the difference in band offsets.

Since Fig. 3 shows some Fe character in the top 0.4–0.6 eV of the valence band of the interfacial superlattices, but the interior layer of the $Fe_2O_3$ region carries no weight in that energy range, it follows that the interfacial or near-interfacial $Fe_2O_3$ layers must account for the Fe character at those energies, hence, these layers must have a different electronic structure than the bulk-like interior layers. Accordingly, in Fig. 5 we have decomposed the total density of states for the complete interfacial supercells into layer-projected DOS for all the symmetry-distinct layers in the cell (continuing to define "layers" as was done for Fig. 4). Figure 5(a) shows the DOS for six layers (three hematite, three chromia) spanning one of the O-divided interfaces, the other interface being related to the one shown by symmetry. Figure 5(b) displays the layer-projected DOS for seven layers spanning the ferromagnetic split-metal interface, i.e., the one near the center in the right-hand cell in Fig. 1. The extra layer is the mixed "$FeCrO_3$" layer at the interface itself, with the adjacent layers now designated as "near-interface." (The total number of layers is still the same, since there is now only one "interior" layer in each bulk-like region, instead of two interior layers related by symmetry as in the oxygen-divided supercell.) Comparing Figs. 5(a) and 5(b), an important difference emerges between the two different interfaces: in the O-divided system the states near the edges of the fundamental band gap (dotted lines in Fig. 4) are strongly concentrated on the interfacial layers, while in the split-metal system the band edge states are mostly in the intermediate and interior layers. To put it differently, in the O-divided case there appear to be interfacial states extending slightly into the "bulk" gap, while any interfacial states in the split-metal superlattice are well within the bulk-like energy ranges of the band structure. Figure 5(b) shows this behavior of the ferromagnetic split-metal interface only, but we have confirmed that the layer density of states has a similar behavior at the antiferromagnetic split-metal interface also. This behavior has implications for charge separation, as we discuss below.
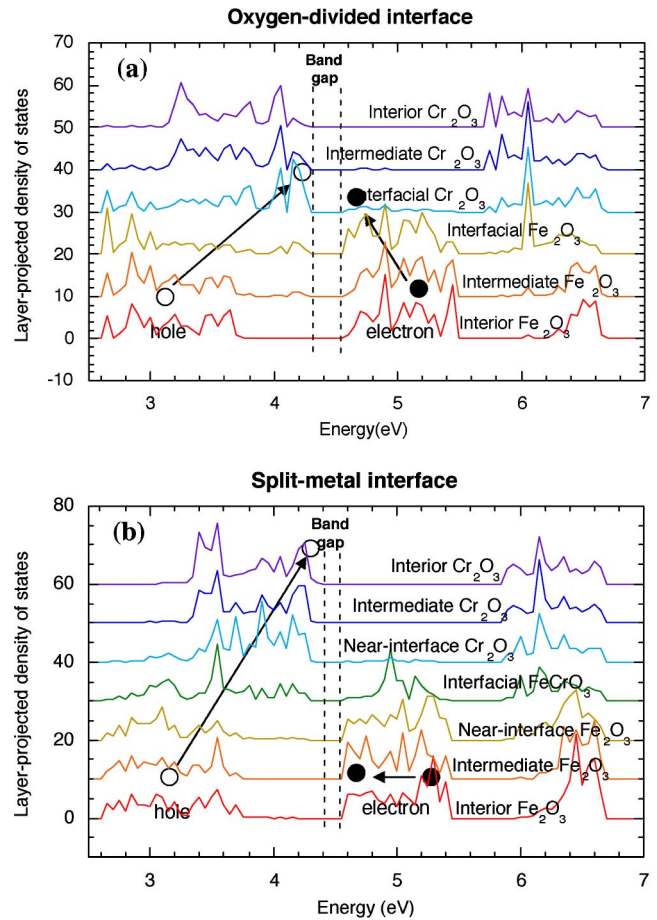


FIG. 5. (Color online) Layer-by-layer projected density of states for (a) oxygen-divided interface and (b) ferromagnetic split-metal interface. "Layers" are defined as in the caption to Fig. 4 and labeled in Fig. 1. Relaxation of photoexcited electrons and holes to the band edges is schematically indicated, with the finals states on interfacial layers in (a) and interior layers in (b).

## V. DISCUSSION AND PREDICTIONS

A key point is whether we can identify our O-divided and split-metal interfaces with, respectively, the $Fe_2O_3$-on-top and $Cr_2O_3$-on-top interfaces of Chambers *et al.*,[2] such as would lead to a reasonable agreement between theory and experiment. In this regard some recent experimental evidence may be relevant. The (0001) face of both of these oxides is usually terminated by a metal layer, having the form of the "lower half" of one of our bilayers; this termination ensures that a nonpolar surface results, thus minimizing the electrostatic energy of the surface. If we stop growing one oxide with such a termination, then start growing the other epitaxially, a split-metal interface would likely ensue. However, with $Cr_2O_3$, but apparently not with $Fe_2O_3$, it is also possible to have the (0001) surface terminated by an oxygen plane (achieved by growth at higher $O_2$ partial pressure.)[13,14] Thus, the $Fe_2O_3$-atop-$Cr_2O_3$ *may* correspond to the oxygen-divided interface we have discussed, while the $Cr_2O_3$-atop-$Fe_2O_3$ interface probably is a split-metal interface. Since the $Fe_2O_3$-atop-$Cr_2O_3$ interface must somehow differ from the $Cr_2O_3$-atop-$Fe_2O_3$ interface in order to have a

different valence band offset, we propose that the $Fe_2O_3$-atop-$Cr_2O_3$ interface is indeed the O-divided interface of our calculation. If we are correct, then our predictions are in reasonable agreement with experiment: the valence band offset is 0.4 eV (calculated) vs. $0.3 \pm 0.1$ eV (experiment)[2] for the O-divided interface, and 0.6 eV vs. $0.7 \pm 0.1$ eV[2] for the split-metal interface.

The ability to controllably produce two different interfaces, with different band offsets, in the same crystallographic plane between a pair of materials has interesting implications for charge separation in a photovoltaic or photochemical device. A superlattice with several consecutive repeats could be grown with the two interfaces alternating, such as to create an electrochemical potential gradient that would sweep electrons and holes in opposite directions.[2] However, carrier lifetimes must also be considered, and the electronic structure of the interfaces studied here has consequences for electron-hole recombination. Consider the fate of an electron-hole pair excited in the hematite region, with the hole initially in the complex of Fe $3d$-dominated states about 1.5 eV below the valence band maximum, and the electron initially in the Fe $3d$ states just above the conduction band minimum. The electron will simply relax down in energy to the conduction band edge, while the hole works its way upwards into the occupied states of Cr $3d$ character. This it can do because there are many overlapping Fe and Cr states, including interfacial states, around 1 eV below the valence band edge.

But now consider what happens to the hole as it approaches the valence band maximum. In the oxygen-divided system, the band edge states have strong interfacial character, so the hole will tend to localize near the interface, as will the electron in the conduction band. Recombination is then likely to occur, frustrating any attempt to exploit the energy in the electron-hole excitation. However, in the split-metal system the band edges have interior-layer character, with the interfacial states pushed away from the band edges. The electron and hole thus tend to avoid the interfacial layer when they relax, respectively, to the conduction band minimum and valence band maximum. Thus, we predict that recombination will be inhibited at the split-metal interface, in comparison to the O-divided interface. This property could be important for photonic device design based on the (0001) interfaces between hematite and chromia.

## VI. SUMMARY

In this work we have studied two possible structures for the interface between $\alpha$-$Cr_2O_3$ and $\alpha$-$Fe_2O_3$ in the hexagonal (0001) plane. By a version of the usual first-principles approach based on reference electrostatic potential shifts, we have shown that these structures lead to significantly different values of the valence band offset. One of the two interface structures, the split-metal structure, is predicted to be significantly better than the other at preventing electron-hole recombination. The two interfaces are close enough in energy that details of epitaxial growth procedures and kinetic considerations will likely control which one actually forms, as indeed appears to be the case experimentally. Complex magnetic properties may be found in superlattices of these interfaces. Moreover, chemical modifications of the interfacial layer strongly affect the band offset value. These more recent results will be considered in our future work.[15]

*Author to whom correspondence should be addressed. Email address: maciej.gutowski@pnl.gov

[1] P. A. Cox, *Transition Metal Oxides: An Introduction to Their Electronic Structure and Properties* (Clarendon, Oxford, 1992).

[2] S. A. Chambers, Y. Liang, and Y. Gao, Phys. Rev. B **61**, 13223 (2000).

[3] X.-G. Wang, W. Weiss, Sh. K. Shaikhutdinov, M. Ritter, M. Petersen, F. Wagner, R. Schlögl, and M. Scheffler, Phys. Rev. Lett. **81**, 1038 (1998); E. R. Battista and R. A. Friesner, J. Phys. Chem. B **106**, 8136 (2002).

[4] C. Rehbein, N. M. Harrison, and A. Wander, Phys. Rev. B **54**, 14066 (1996).

[5] Y. Wang and J. P. Perdew, Phys. Rev. B **43**, 8911 (1991); **44**, 13298 (1991); J. P. Perdew, in *Electronic Structure of Solids '91*, edited by P. Ziesche and H. Eschrig (Akademie Verlag, Berlin, 1991).

[6] G. Kresse and J. Hafner, Phys. Rev. B **47**, 558 (1993); **48**, 13115 (1993); **49**, 14251 (1994); J. Phys.: Condens. Matter **6**, 8245 (1994); G. Kresse and J. Furthmüller, Comput. Mater. Sci. **6**, 15 (1996); Phys. Rev. B **54**, 11169 (1996).

[7] D. Vanderbilt, Phys. Rev. B **41**, 7892 (1990).

[8] S.-H. Wei and A. Zunger, Appl. Phys. Lett. **72**, 2011 (1998) and references therein.

[9] J. E. Jaffe and M. Gutowski (unpublished).

[10] J. B. Goodenough, in *Progress in Solid State Chemistry, v. 5*, edited by H. Reiss (Pergamon, Oxford, 1971), p. 145ff.

[11] The hexagonal lattice constants of the corundum structure are related to the rhombohedral primitive ones by $a = a_{rhomb}[2(1 - \cos\alpha)]^{1/2}$, $c = a_{rhomb}[3(1 + 2\cos\alpha)]^{1/2}$.

[12] S. A. Chambers and J. R. Williams, private communication.

[13] S. A. Chambers and S. I. Yi, Surf. Sci. **439**, L785 (1999).

[14] S. A. Chambers, in *The Chemical Physics of Solid Surfaces, v. 9: Oxide Surfaces*, edited by D. P. Woodruff (Elsevier, Amsterdam, 2001), p. 301.

[15] M. Gutowski and J. E. Jaffe (unpublished).